Supplementary Information

Structure of the PCNA-p15^{PAF} complex and implications for clamp sliding on the DNA during replication and repair

Alfredo De Biasio, Alain Ibáñez de Opakua, Gulnahar B. Mortuza, Rafael Molina, Tiago N. Cordeiro, Francisco Castillo, Maider Villate, Nekane Merino, Sandra Delgado, David Gil, Irene Luque, Tammo Diercks, Pau Bernadó, Guillermo Montoya, Francisco J. Blanco

Supplementary Figures:

Supplementary Figure 1. Isothermal titration calorimetry measurements and analysis of p15 and fragments binding to PCNA.

Supplementary Figure 2. NMR spectra of PCNA bound to p15 and three p15 fragments.

Supplementary Figure 3. Chemical shift perturbations (CSP) measured for PCNA bound to p15 and its fragments.

Supplementary Figure 4. Chemical shift perturbations (CSP) of PCNA backbone amide ^{1}H and ^{15}N NMR resonances caused by binding of p15 or its fragments.

Supplementary Figure 5. Crystal contacts at the p15$^{50-77}$-free PIP-box binding site on the PCNA trimer.

Supplementary Figure 6. Stereo view of the refined $2F_0$-F_c map corresponding to the location of p15$^{50-77}$ bound to PCNA.

Supplementary Figure 7. Scheme of the interactions between p15$^{50-77}$ and PCNA in the crystal structure of the complex, analyzed and depicted with LIGPLOT.

Supplementary Figure 8. NMR titration of PCNA with p15 and aggregation test on the p15-PCNA complex.

Supplementary Figure 9. Quantitative NMR intensity analysis of selected PCNA signals in the presence of substoichiometric amounts of p15 or $p15^{50-77}$.

Supplementary Figure 10. NMR analysis of PCNA interaction with the short primed DNA.

Supplementary Figure 11. Fluorescence polarization measurements of p15 binding to different DNA molecules.

Supplementary Figure 12. NMR analysis of p15 binding to a 24 bp DNA duplex in low and medium salt buffers.

Supplementary Figure 13. CSP of p15 NMR signals caused by dsDNA binding in medium salt buffer.

Supplementary Figure 14. Contact van der Waals energy versus RMSD of the binding interface calculated for the 20 models of the ternary complex p15-PCNA-DNA.

Supplementary Figure 15. Gallery of all class averages from the 2D reference-free alignment of individual particles seen by electron microscopy in p15-PCNA, p15-PCNA-DNA and PCNA-DNA samples with negative staining.

Supplementary Figure 16. Harmonic analysis of individual particles seen in electron micrographs and used for classification by the KerDenSOM method.

Supplementary Figure 17. Sequence alignment of the N-terminal regions of p15 proteins and histone H3.

Supplementary Tables:

Supplementary Table 1. Thermodynamic parameters of the binding of p15 molecules to PCNA at two different temperatures as measured by ITC.

Supplementary Table 2. Sequences of the oligonucleotides used for the DNA binding experiments.

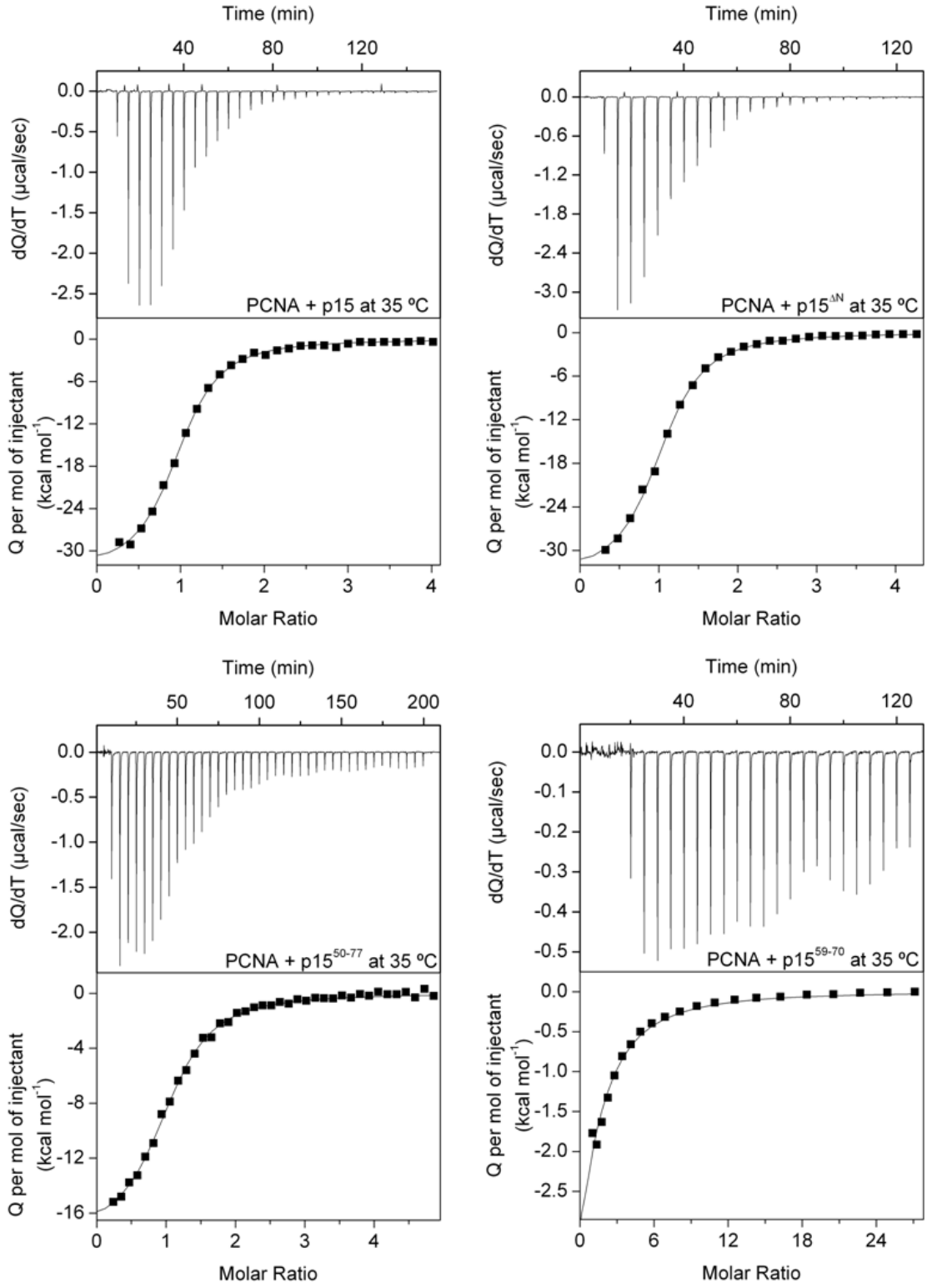

Supplementary Figure 1. Isothermal titration calorimetry measurements and analysis of p15 and fragments binding to PCNA in PBS, pH 7.0 at 35 °C. All data were fitted to a binding model assuming equivalent sites on PCNA. The derived thermodynamic parameters are listed in Supplementary Table 1.

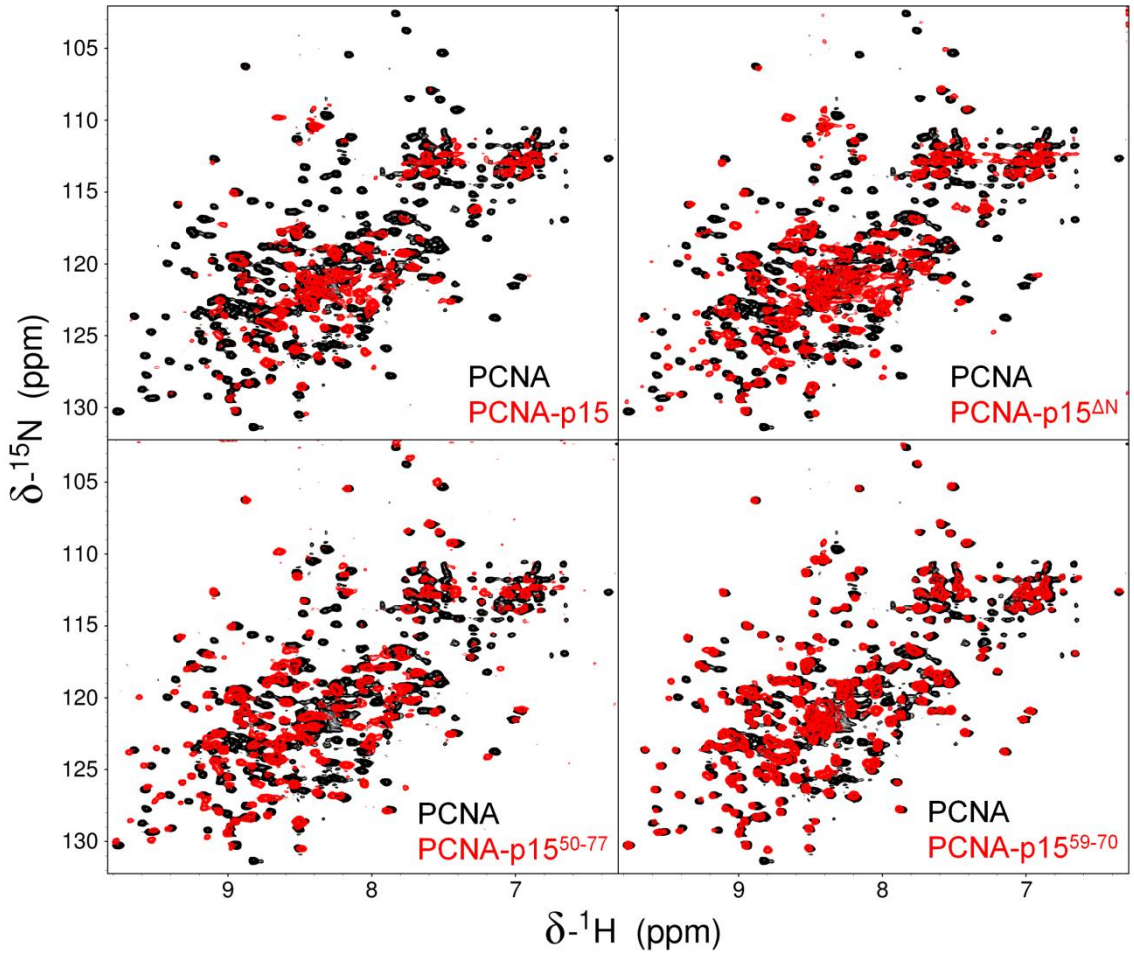

Supplementary Figure 2. NMR spectra of PCNA bound to p15 and its fragments. Superposition of ^{1}H-^{15}N TROSY spectra of 50 µM U-[^{2}H,^{15}N]-PCNA in the absence (black) and presence (red) of 250 µM full-length p15, p15$^{\Delta N}$, p15$^{50-77}$, or 165 µM p15$^{59-70}$, as indicated. The spectrum in the presence of p15$^{59-70}$ was recorded with 98 points in the indirect dimension while the others were recorded with 128 points. All spectra were acquired at 35 °C on samples in PBS, pH 7.0, 1 mM DTT. Superposed spectra were plotted with identical or comparable contour levels to highlight differences in signal intensities. The strong reduction observed for some signals of perdeuterated PCNA in the presence of non-deuterated full length p15 is likely due not only to the increase in the size of the complex and in proton density around the PCNA amide protons, but mainly to line broadening and signal dilution caused by transient and conformationally heterogeneous interactions with the disordered p15 termini.

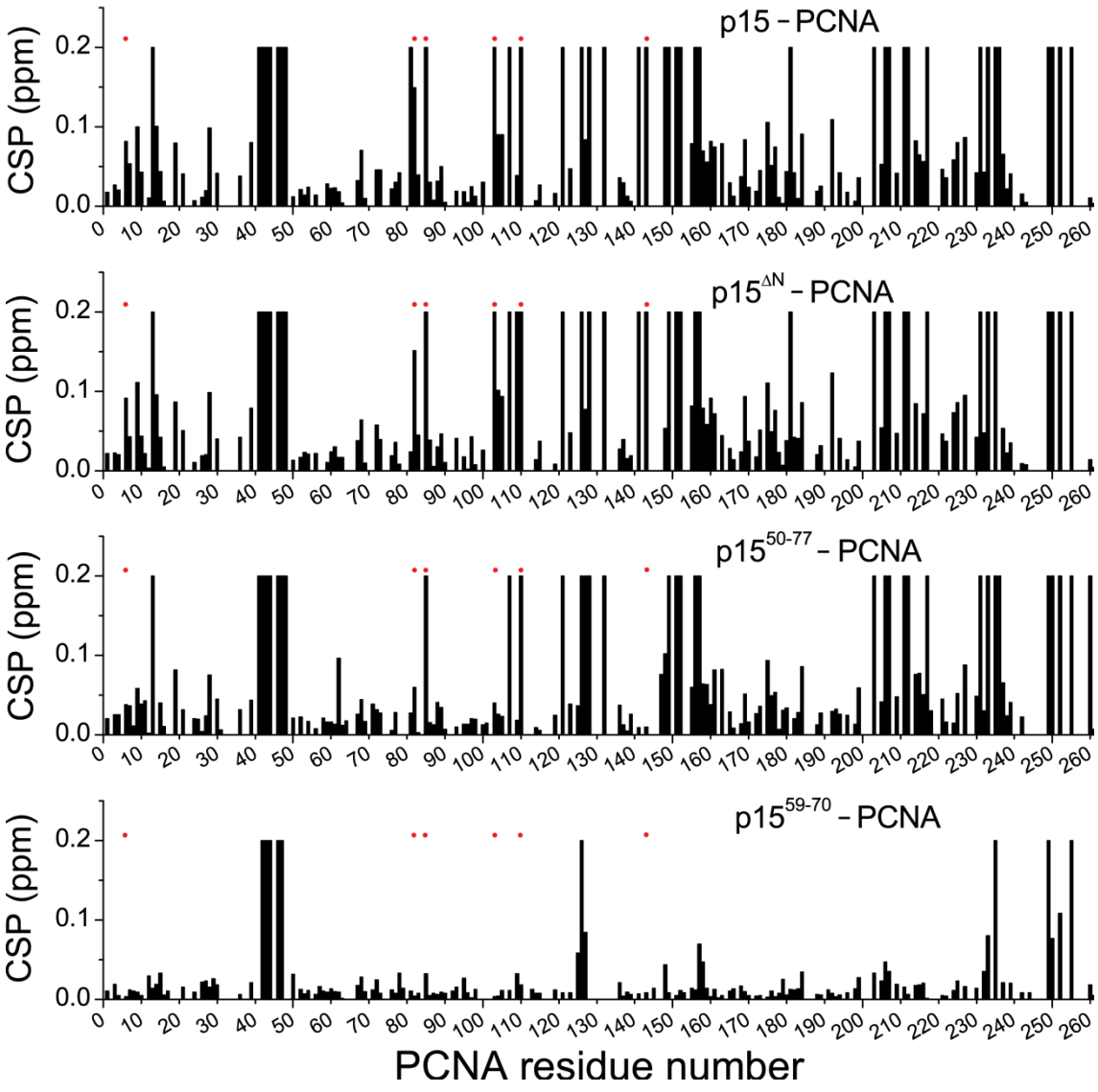

Supplementary Figure 3. Chemical shift perturbations (CSP) of PCNA backbone amide ^{1}H and ^{15}N NMR resonances caused by binding of p15 or its fragments. Tentative assignments of p15-bound PCNA were deduced from the NMR titration of PCNA with p15 (Supplementary Figure 8a). This assignment was transferred to PCNA bound to the p15 fragments based on nearest neighborhood comparison, and was facilitated by the joint examination of all four complex spectra. The assignments cover 44, 44, 48 and 59 % of the non-proline PCNA residues bound to p15, $p15^{\Delta N}$, $p15^{50-77}$, or $p15^{59-70}$, respectively. Resolved signals in the free form whose bound form could not be assigned (due to signal disappearance along the titration with p15) were classified as perturbed and a CSP of 0.2 ppm was used to represent their perturbation in the plot. This value was chosen based on the range of CSP measured for PCNA in complex with a short PIP fragment of p21 (reference no. 18). For some residues neither assignment nor classification as perturbed could be made due to signal overlap or very weak signal intensity in the spectrum of free PCNA; these residues represent 41, 41, 38 and 38 % of the non-proline PCNA residues bound to p15, $p15^{\Delta N}$, $p15^{50-77}$, or $p15^{59-70}$, respectively. The red circles indicate the six back-face residues that experience large signal attenuations upon adding full length p15, but not $p15^{50-77}$ (Supplementary Figure 9).

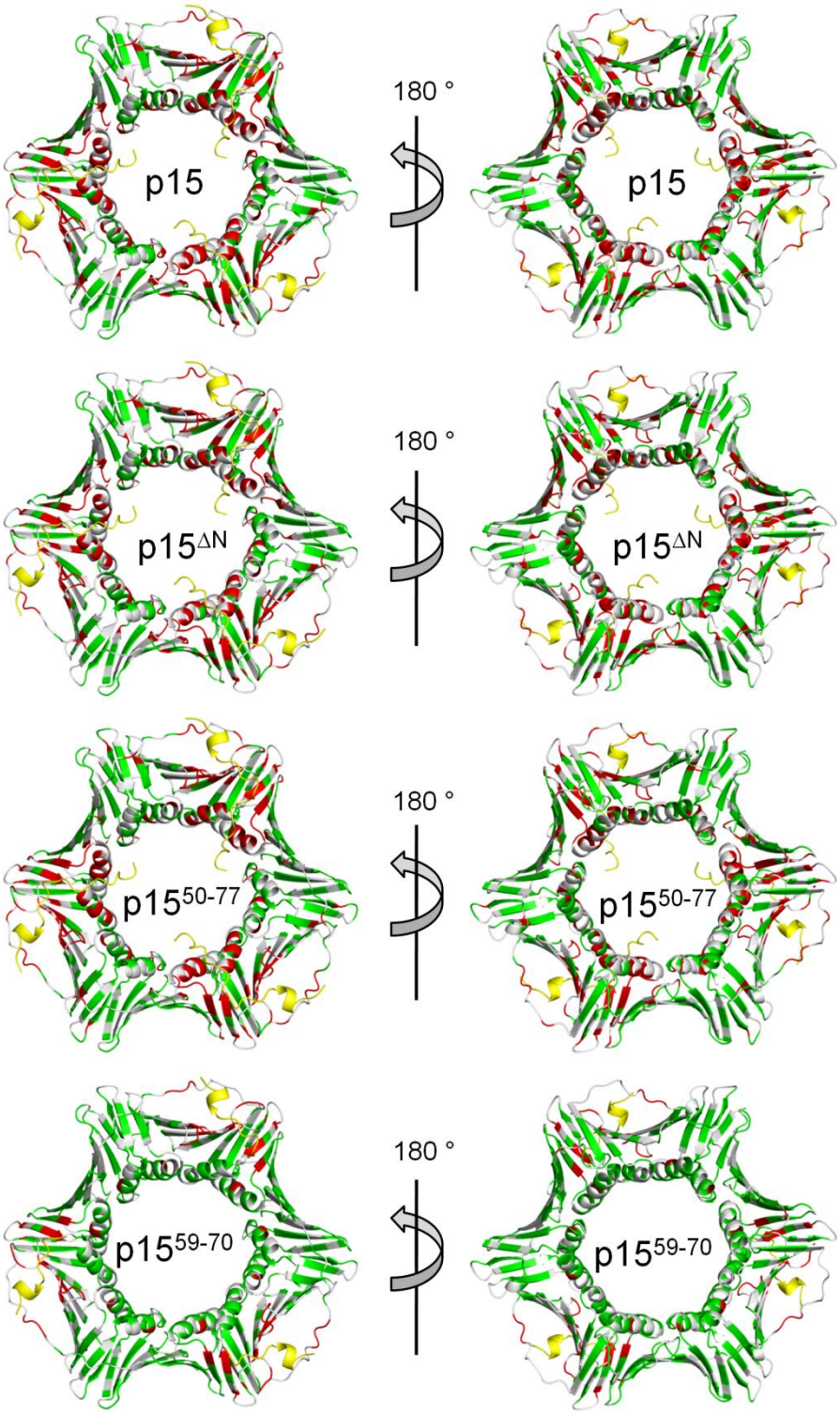

Supplementary Figure 4. Mapping of CSP on the crystal structure of $p15^{50-77}$-PCNA (red for perturbed, green for non-perturbed, and grey for unknown or prolines residues). CSP were considered significant if they were larger than the average plus one standard deviation. The $p15^{50-77}$ residues observed in the electron density are shown in yellow. For the sake of clarity, a third p15 molecule (not seen in the crystal) has been added to the unoccupied protomer, and in the panels showing CSP caused by the short $p15^{59-70}$ peptide, the terminal residues absent in this shorter peptide have been omitted. The left and right panels show the front-face and back-face of the ring, respectively.

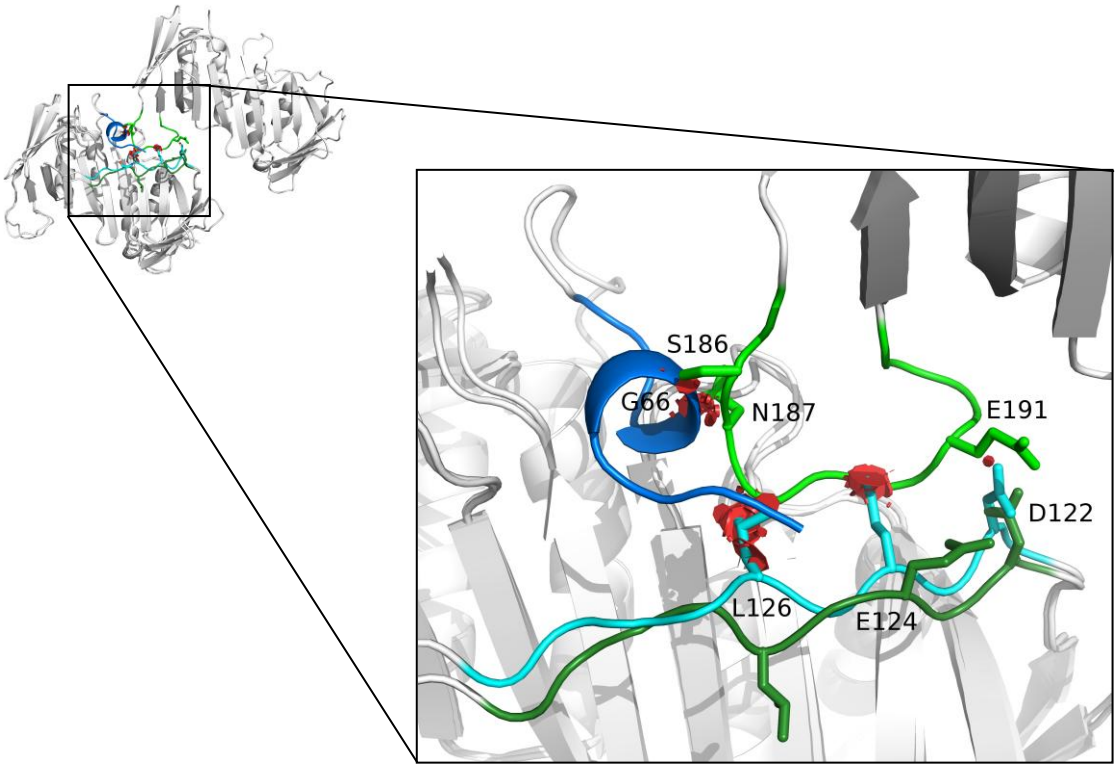

Supplementary Figure 5. Crystal contacts at the p15$^{50-77}$-free PIP-box binding site on the PCNA trimer. The pertaining PCNA protomer (grey ribbon) in our crystal structure of the p15$^{50-77}$-PCNA complex is found to be occluded by a vicinal symmetry-related PCNA protomer. Details of the superposition with a PCNA protomer bound to p15$^{50-77}$ (of which residues around the PIP box including the short 3_{10} helix are shown in blue) are revealed in the zoom. The IDCL loop of the p15$^{50-77}$-free protomer is shown in dark green, that of the p15$^{50-77}$-loaded protomer in cyan, and the loop βD2- βE2 of the vicinal symmetry related PCNA protomer in light green. Red areas indicate van der Waals overlap between both bimolecular interfaces that are avoided in the p15$^{50-77}$-free protomer by local conformational changes at the indicated IDCL residues.

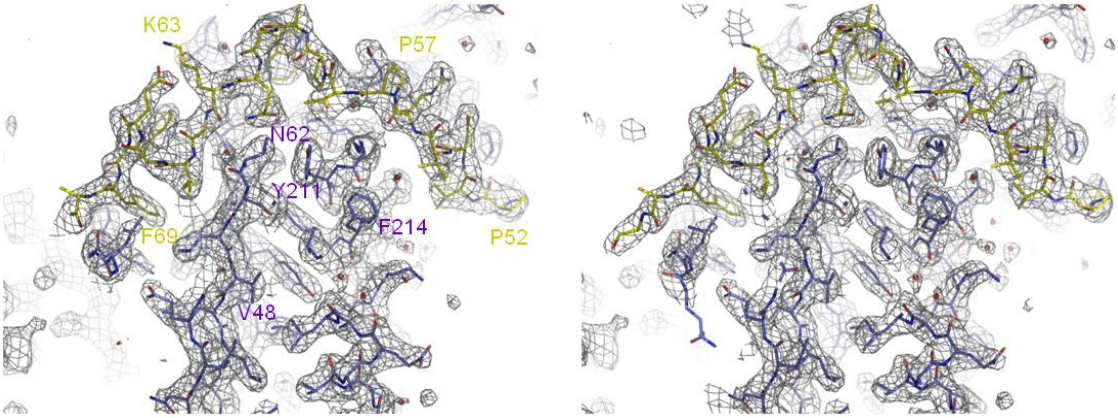

Supplementary Figure 6. Stereo view of the refined $2F_0$-F_c map at the $p15^{50-77}$-PCNA interface. The map is displayed at a contour level of 1.0 σ. PCNA and p15 chains are shown as sticks with carbon atoms in violet and yellow, respectively. Some PCNA and $p15^{50-77}$ residues are labeled.

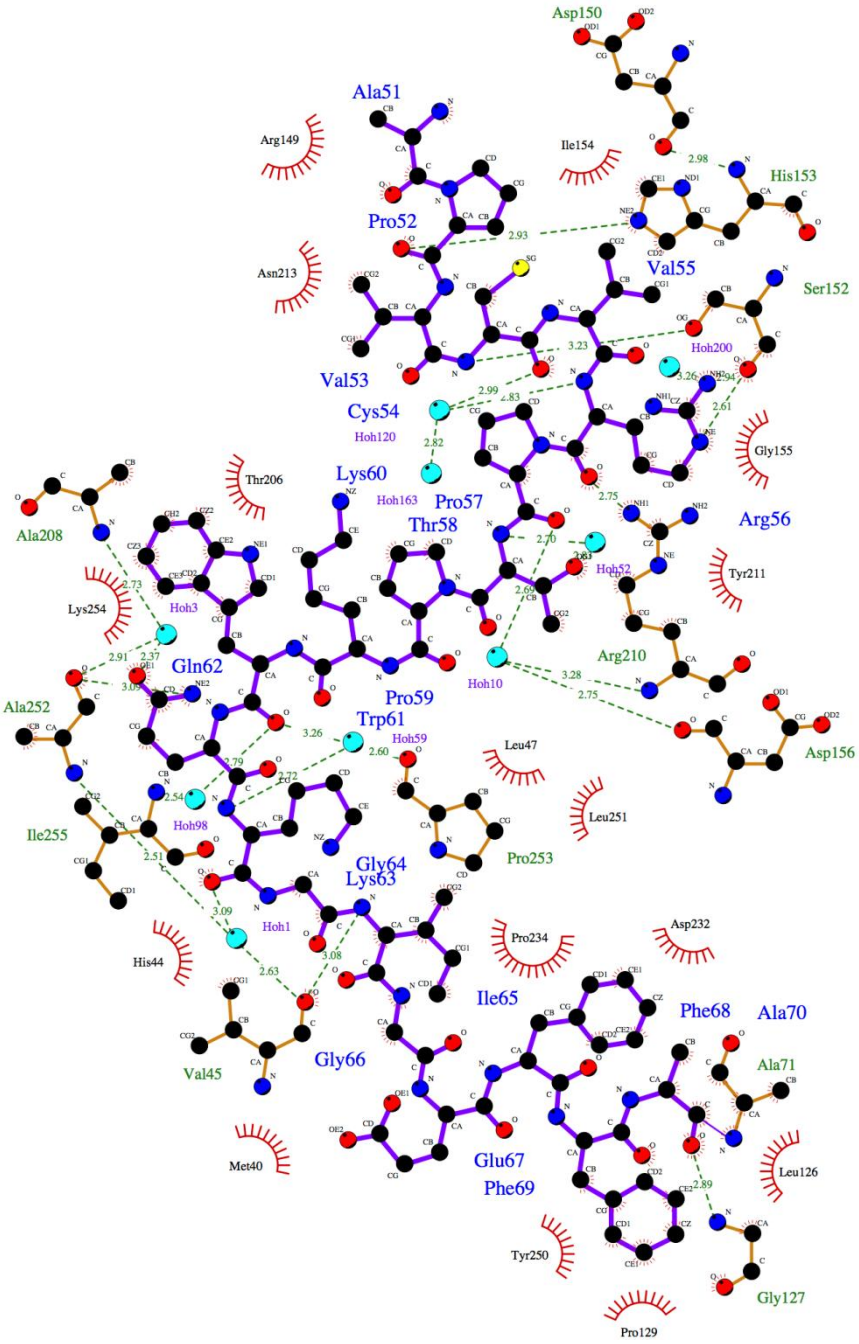

Supplementary Figure 7. Scheme of the interactions between $p15^{50-77}$ and PCNA in the crystal structure of the complex, analyzed and depicted with LIGPLOT (https://www.ebi.ac.uk/thornton-srv/software/LigPlus/). Shown are the interactions between chain D ($p15^{50-77}$, ball-and-stick representation with purple bonds and blue labels) and chain C (PCNA, orange bonds and green or black labels). Carbon, nitrogen and oxygen atoms are colored black, blue and red, respectively. Oxygen atoms of water molecules are colored cyan. Polar interactions are indicated by dotted green lines along with their interatom distances; non-bonded contacts are indicated by red spoked arcs around the involved atoms or residues. Not identified by LIGPLOT but detected by CaPTURE (http://capture.caltech.edu), the W61 indole ring of p15 is involved in a cation-π interaction with the K254 sidechain amine group of PCNA. The total buried interface is 2220.4 $Å^2$ (53.1% on $p15^{50-77}$, 46.5% on PCNA), as determined by the Protein Interfaces, Surfaces and Assemblies server (PISA) at the European Bioinformatics Institute (http://www.ebi.ac.uk/msd-srv/prot_int/pistart.html).

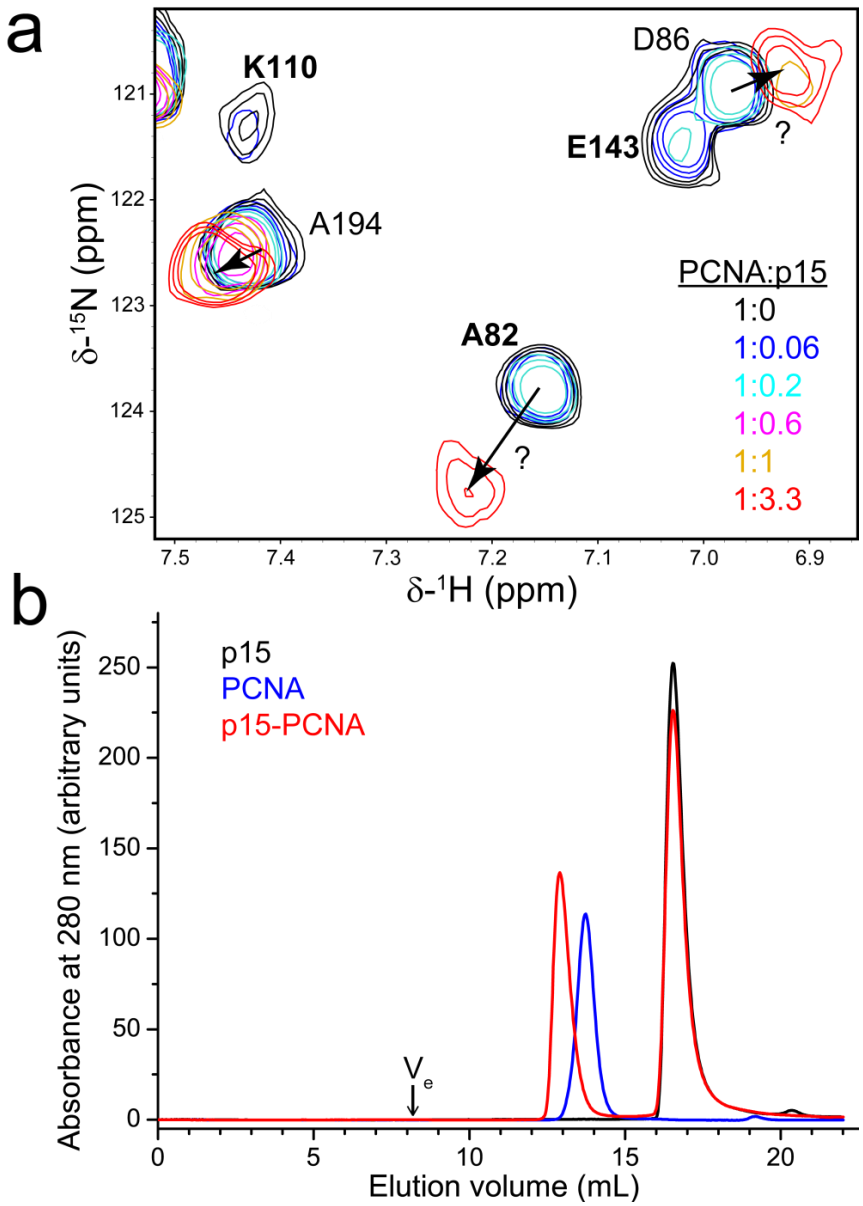

Supplementary Figure 8. NMR titration of PCNA with p15 and aggregation test on the p15-PCNA complex. (**a**) Overlay of ^{1}H-^{15}N- TROSY spectra of 50 μM U-[^{2}H,^{15}N] PCNA after addition of unlabelled p15 at the indicated monomer molar ratios in PBS, pH 7.3 at 35 ºC. The selected region contains resolved signals from residues on the back-face of PCNA that display different behaviors along the titration. The arrows show the deduced signal shifts (only tentative in the case of A82 and D86, as indicated by the question marks). For the sake of clarity a maximum of three contour levels are plotted in each spectrum. Bold labels indicate back-face residues whose signal attenuation at 1:0.2 ratio (with p15 or with p15$^{50-77}$) is quantitatively represented in Supplementary Fig. 9. (**b**) Overlay of size exclusion chromatograms of 250 μM p15 (black), 50 μM PCNA (blue) and a mixture or both (red) in PBS pH 7.4 at room temperature. The arrow indicates the exclusion volume (V_e) of the column.

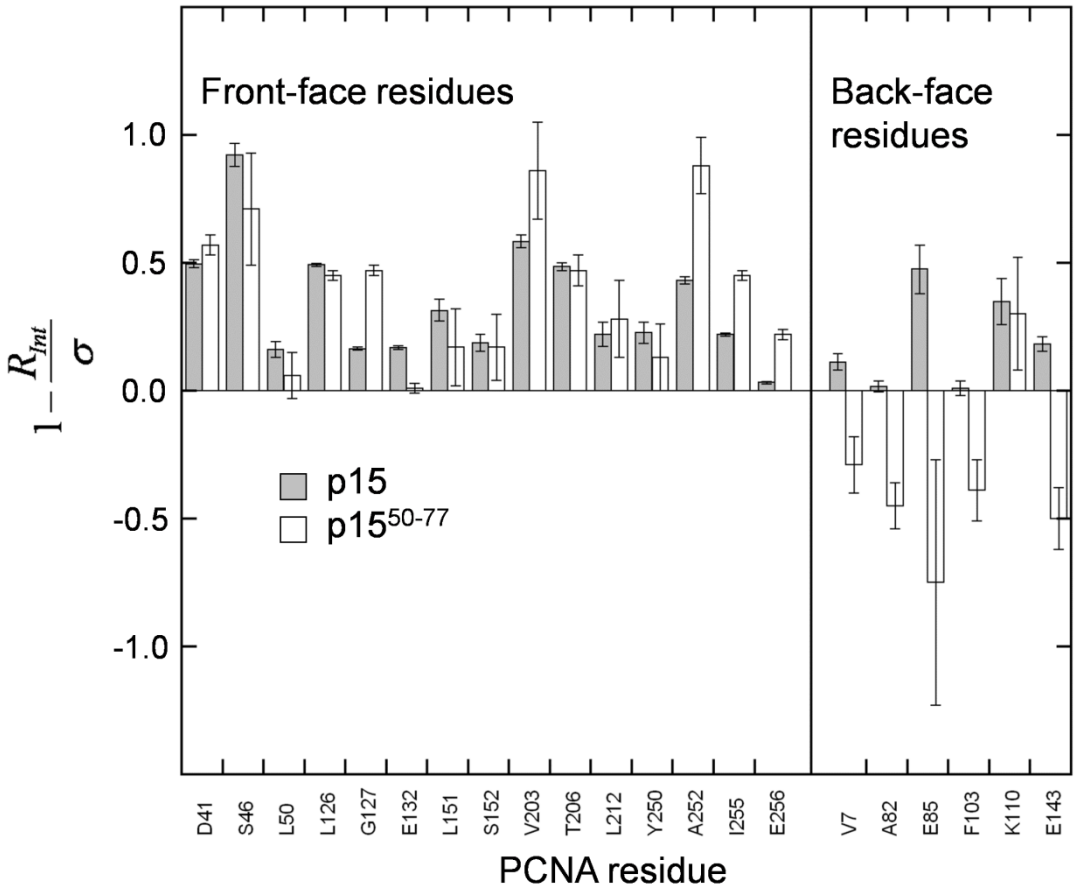

Supplementary Figure 9. Quantitative NMR intensity analysis of selected PCNA signals in the presence of substoichiometric amounts of p15 or p15$^{50-77}$. Intensity analysis of selected well-resolved PCNA ^{1}H-^{15}N TROSY signal. The intensity ratio (R_{Int}) in the presence and absence of full length p15 or p15$^{50-77}$ at 1:0.2 (^{2}H,^{15}N-PCNA:p15 monomer molar ratio, with [PCNA] = 200 μM) are shown as deviations from unity by multiples of the threshold of significance, σ (the mean intensity ratio minus one standard deviation). In this representation, perturbed and unperturbed residues show positive and negative values, respectively. Only those residues on the PCNA front-face that experience a significant intensity drop with both p15 and p15$^{50-77}$ are displayed. On the PCNA back face, contrarily, significant signal attenuations are only observed for full-length p15 (with the possible exception of K110 that also shows perturbation with the truncated p15$^{50-77}$, however, with high uncertainty due to its low signal intensity). The PCNA back-face residues significantly attenuated in the presence of p15 form a nearly contiguous region on the PCNA surface (Figure 3a) involving the N-terminus of helix αA2 on one protomer (E143), and the αA1-βA1 loop (V7), αB1-βG1 loop (A82, E85), βH1 (F103) and βI1 strands (K110) on the adjacent protomer.

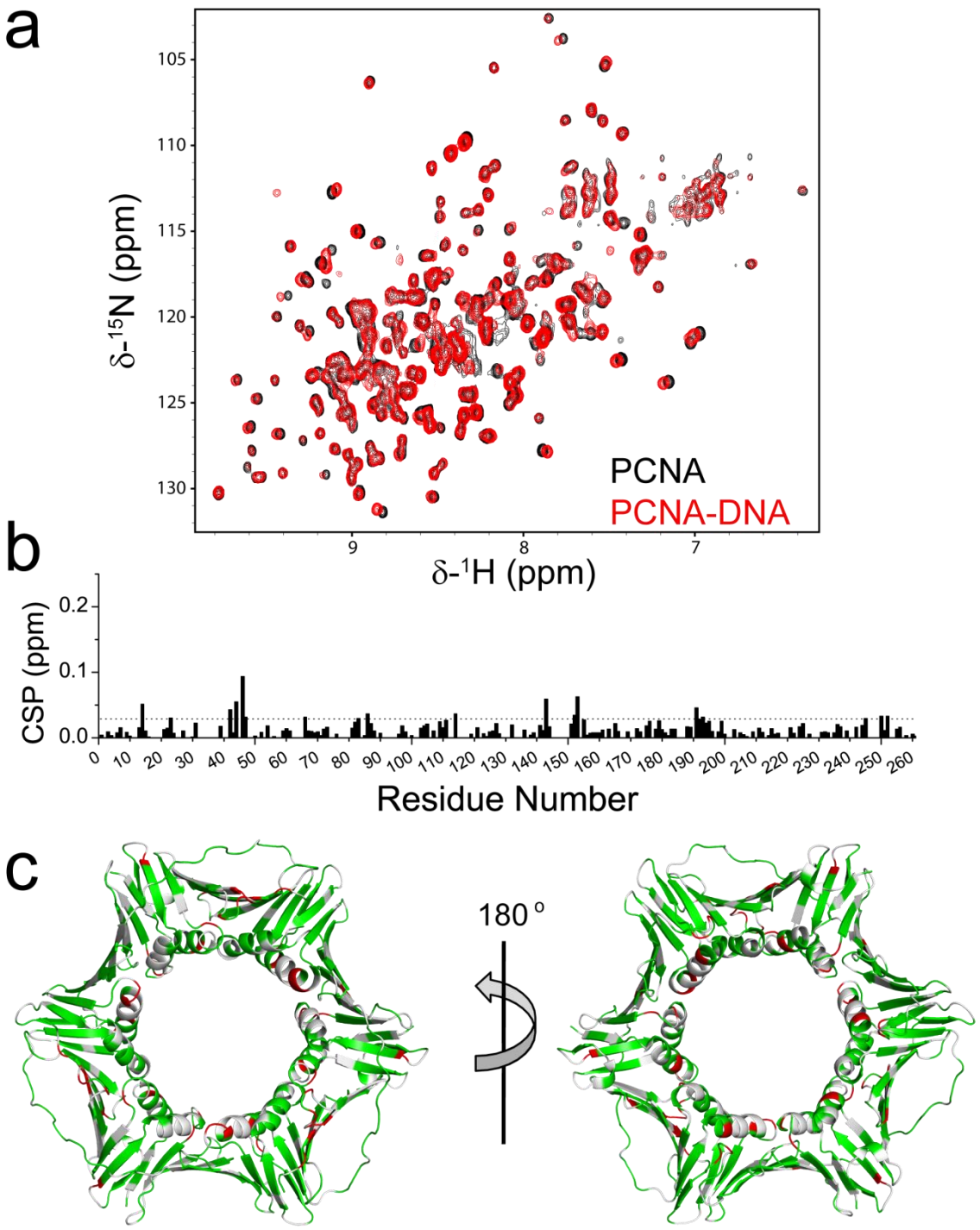

Supplementary Figure 10. NMR analysis of PCNA interaction with the short primed DNA. (**a**) Superposition of ^{1}H-^{15}N TROSY spectra of 50 µM U-[^{2}H,^{15}N] PCNA in the absence (black) and presence (red) of 2.5 mM short primed DNA (generated with oligonucleotides 8 and 9 in Supplementary Table 2). The spectra were acquired at 35 °C on samples in PBS, pH 7.0, with 64 points in the indirect dimension. (**b**) Chemical shift perturbations of backbone amide ^{1}H and ^{15}N NMR resonances. The dotted line indicates the average plus one standard deviation, the value above which the corresponding residues were considered perturbed by the DNA. (**c**) Mapping of CSP on the crystal structure of PCNA (PDB:1VYM; red for perturbed, green for non-perturbed, and grey for unknown or proline residues). The left and right panels show the front- and back-face of the ring, respectively.

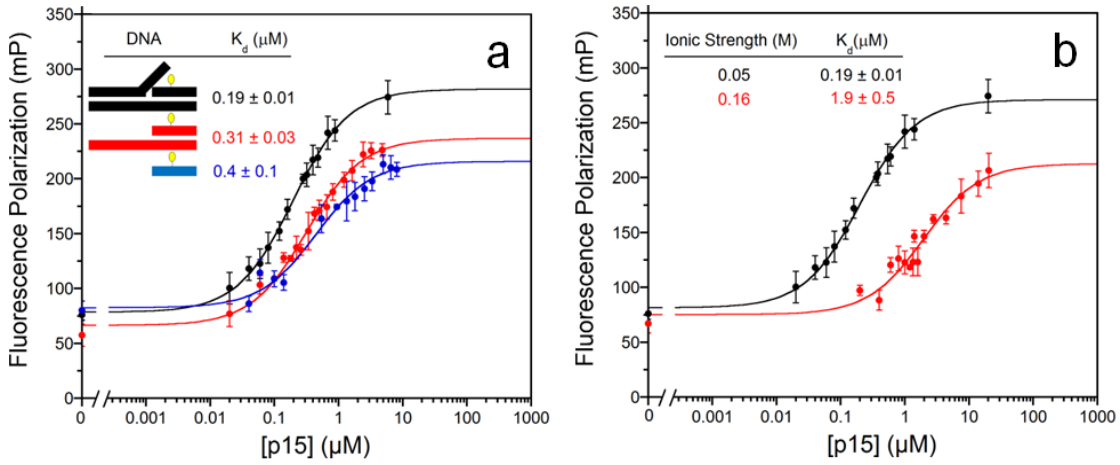

Supplementary Figure 11. Fluorescence polarization measurements of p15 binding to different DNA molecules. (**a**) Binding of p15 to flapped DNA (black), primed DNA (red) and single-stranded DNA (blue) that can be assembled with the oligonucleotides listed in Supplemental Table S2. The yellow circle indicates the attached fluorescent probe. The isotherms (measured at 25 ºC in 30 mM HEPES, pH 7.6, 40 mM KCl, 5% glycerol, 0.1 g/L bovine serum albumin, 2 mM TCEP) were fitted to a single-site binding model yielding the indicated dissociation constants. Since NMR analysis in low salt buffer indicates more than one binding site, the dissociation constants might not correspond to the simple equilibrium used for the fitting and are only apparent constants, but nevertheless indicative of the overall relative DNA affinities. (**b**) Binding of p15 to flapped DNA at 25 ºC in buffers of different ionic strength, as indicated. The data in black are the same as in the left panel. The data in red are measured in PBS (137 mM NaCl, 2.7 mM KCl, 10 mM sodium phosphate, 2 mM potassium phosphate), pH 7.0, 2 mM TCEP. The NMR analysis of the binding in PBS is consistent with one binding site, and the dissociation constants measured by both techniques are on the same order (see Supplementary Figure 12c).

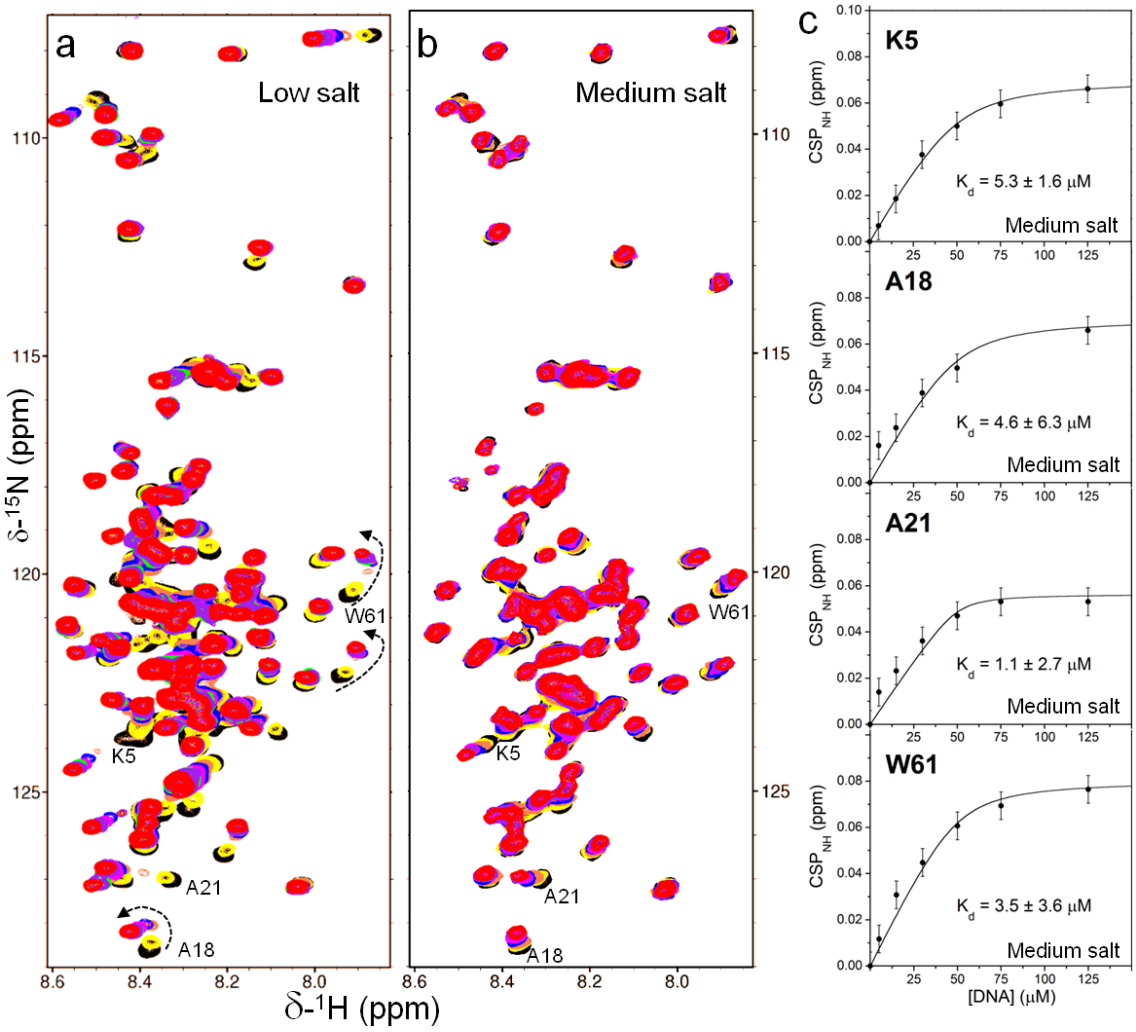

Supplementary Figure 12. NMR analysis of p15 binding to a 24 bp DNA duplex in low and medium salt buffers. All spectra were recorded at 25 ºC. (**a**) Overlay of ^{1}H-^{15}N HSQC spectra of a sample containing 30 μM U-[^{15}N] p15 and 0 to 42 μM dsDNA (colors from black to red) in the low salt buffer 20 mM MES, 1 mM DTT, pH 6.1. Non-linear (curved) signal shifting of some residues is indicated with dotted arrows. (**b**) Overlay of spectra of a sample containing 50 μM U-[^{15}N] p15 and 0 to 125 μM dsDNA in PBS (137 mM NaCl, 2.7 mM KCl, 10 mM sodium phosphate, 2 mM potassium phosphate), 1 mM DTT, pH 6.3. Observed signal shifts here are linear throughout, and residues with relatively large CSP are labeled. (**c**) Analysis of the linear CSP of selected residues in the medium salt buffer spectra using a single-site binding model. Bars represent experimental errors (± 0.006 ppm) while K_d errors are derived from the fitting procedure. These errors are large due to the small signal shifts and large concentration of p15 protein in the samples (about ten times larger than the K_d). Nevertheless, the K_d derived from the four selected residues are on the same order and similar to the K_d measured by fluorescence polarization (K_d = 1.9 ± 0.5 μM; Supplementary Figure 11b).

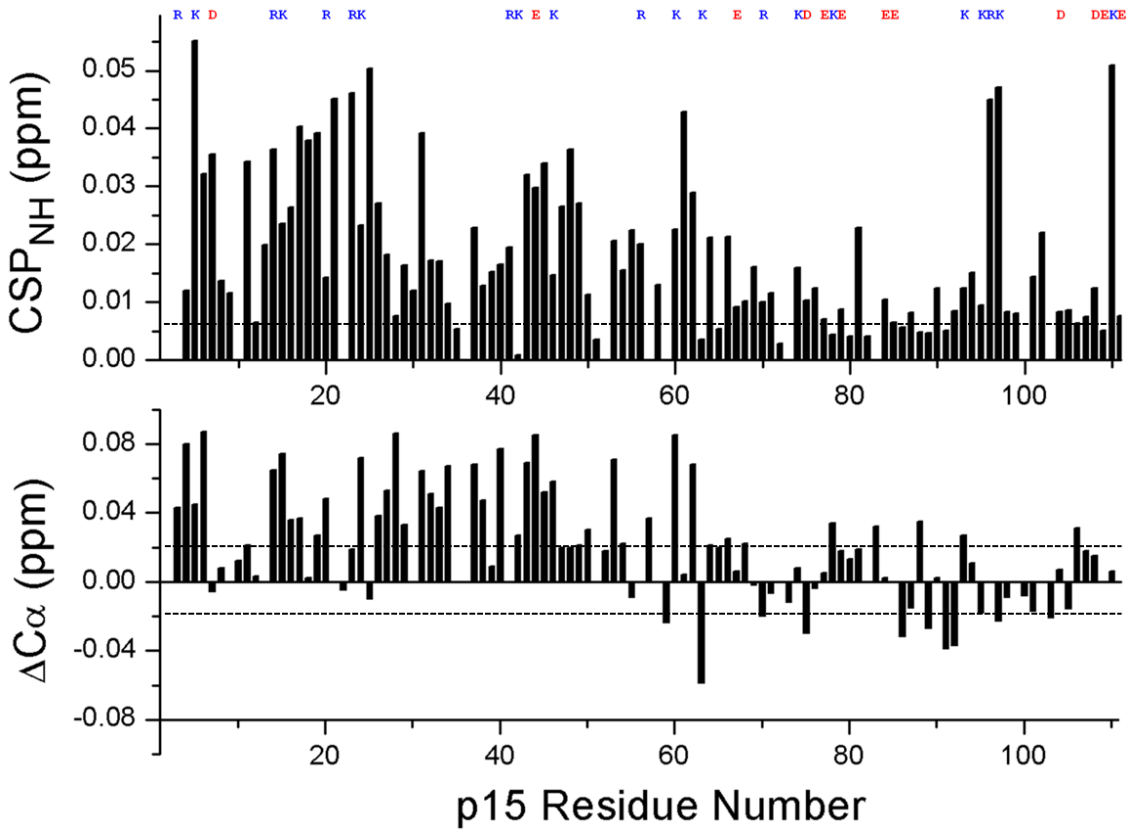

Supplementary Figure 13. CSP of p15 NMR signals caused by dsDNA binding in medium salt buffer (PBS, pH 6.3). The CSP of backbone amide ^{1}H and ^{15}N NMR resonances (**top**) and differences in $^{13}C^{\alpha}$ chemical shifts (**bottom**) are derived by comparing initial and final points of the dsDNA titration (Supplementary Figure 12b) and represented against the p15 residue number. Dotted lines indicate the experimental errors estimated from the digital resolution of the spectra. Above the plot, charged residues in the p15 sequence are indicated in blue and red for positive and negative charges, respectively.

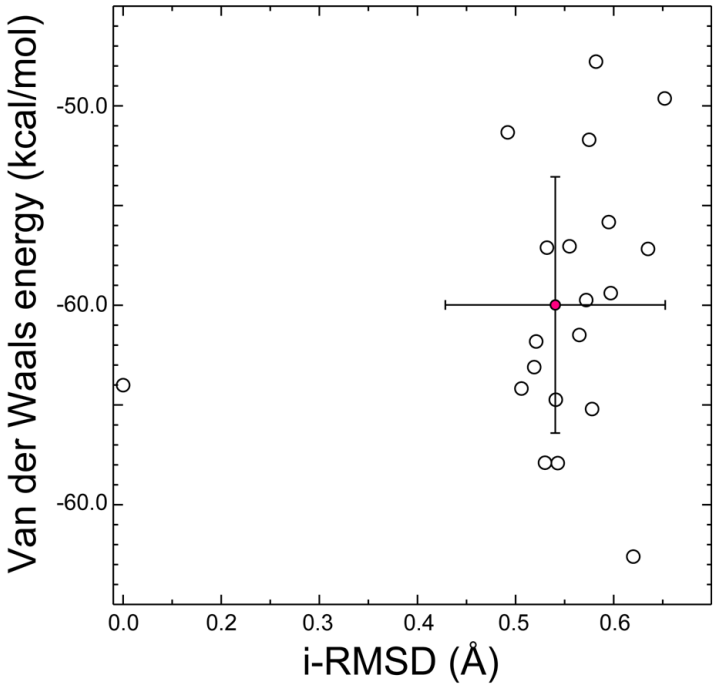

Supplementary Figure 14. Van der Waals contact energy versus RMSD of the binding interface (i-RMSD, with respect to the lowest total energy model) calculated for the 20 models of the ternary complex p15-PCNA-DNA. The i-RMSD was calculated for the backbone heavy atoms of all amino acids (N^H, C^α, C') and nucleotides (O3', C3', C4', C5', O5', P) at intermolecular distances shorter than 10 Å. The red circle corresponds to the mean values, and error bars to the standard deviations.

Statistics of the ensemble of 20 models:

i-RMSD from the lowest energy model = 0.44 ± 0.11 Å,

van der Waals energy = -59.9 ± 3.2 kcal/mol,

electrostatic energy = -666.4 ± 37.8 kcal/mol,

desolvation energy =23.09 ± 3.6 kcal/mol,

buried surface area =1985.1 ± 45.9 $Å^2$.

p15-PCNA

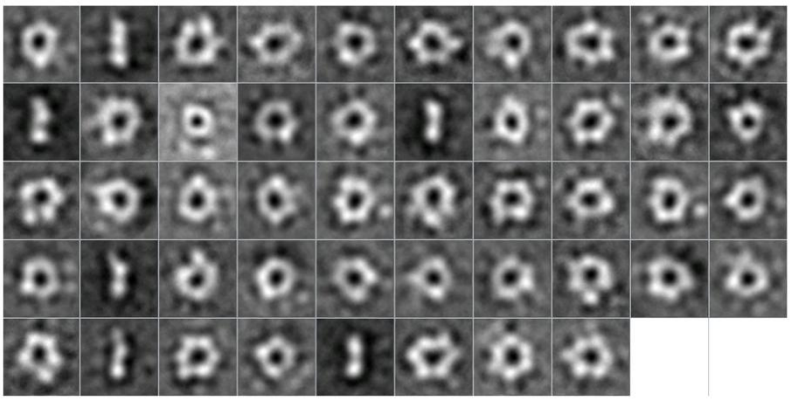

p15-PCNA-DNA

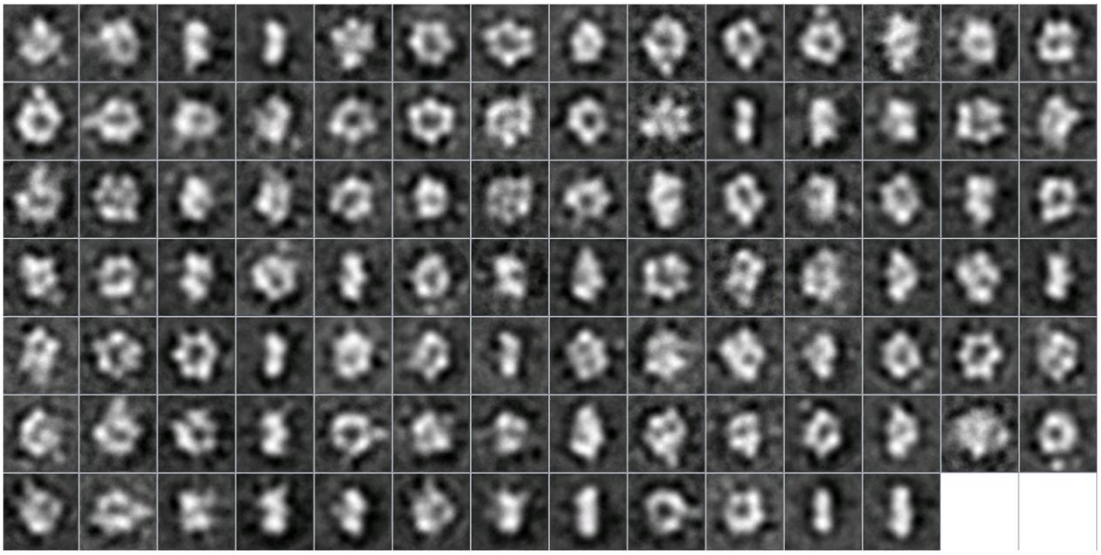

PCNA-DNA

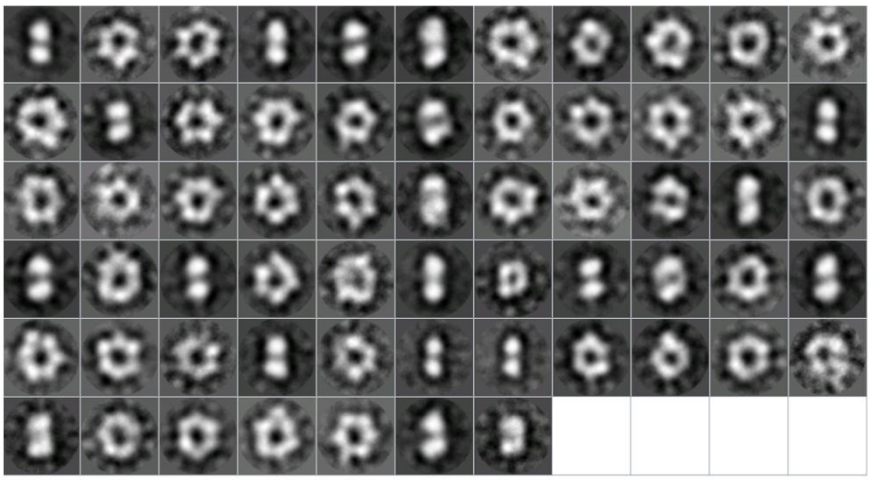

Supplementary Figure 15. Gallery of all class averages from the 2D reference-free alignment of individual particles seen by electron microscopy in p15-PCNA, p15-PCNA-DNA and PCNA-DNA samples with negative staining.

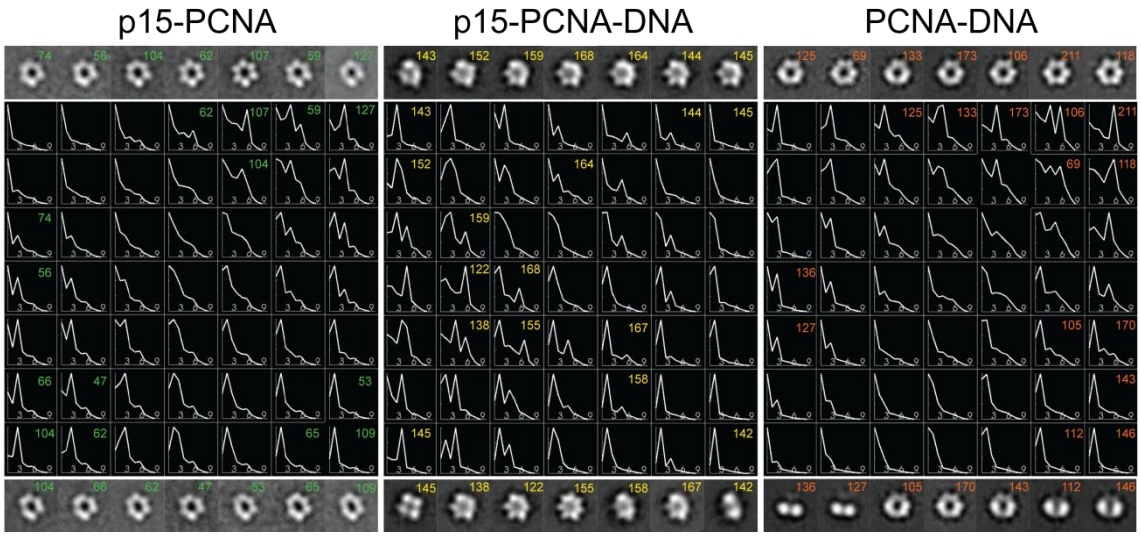

Supplementary Figure 16. Harmonic analysis of PCNA particles seen in electron micrographs of the indicated samples and used for classification by the Kernel Probability Density Estimator Self-Organizing Map (KerDenSOM) method. Plots of the 7×7 results from classifying the rotational power spectra of each individual particle of the three indicated mixtures. Some representative 2D class averages of different projections showing predominant harmonics of order 2, 3 or 6 are displayed above and below the galleries, with the number of individual particles in each cluster indicated. The clusters with harmonics of order 3 and 6 contain predominantly top-view particles, while clusters with harmonic of order 2 contain predominantly side-view particles.

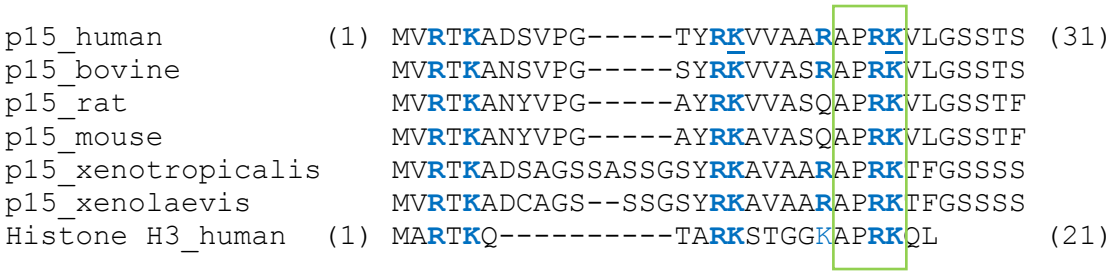

Supplementary Figure 17. Sequence alignment of the N-terminal regions (residue numbers as indicated) of p15 proteins and histone H3. The selected p15 proteins are taken from the Uniprot data base, with entry codes Q15004 (human), Q5E9B2 (bovine), Q6RIA2 (rat), Q9CQX4 (mouse), Q6AZL2 (*X. tropicalis*), Q5HZL4 (*X. laevis*). Histone H3 Uniprot entry is code P68431 (human). Basic residues are colored blue; the green rectangle indicates the common APRK sequence motif. Underlined residues in human p15 are K15 and K24 that become ubiquitylated upon UV-irradiation.

Supplementary Table 1. Thermodynamic parameters of the binding of p15 molecules to PCNA at two temperatures as measured by ITC in PBS, 2mM TCEP, pH 7.0.

p15 molecule	Temperature (ºC)	K_d [a] (μM)	K_a [b] ($10^5 \cdot M^{-1}$)	ΔG[c] (kcal/mol)	ΔH[d] (kcal/mol)	$-T\Delta S$[e] (kcal/mol)	N[f]
p15	25	1.1 ± 0.1	9.5 ± 0.9	-8,20 ± 0.06	-24.2 ± 0.3	16.0 ± 0.4	0.93 ± 0.01
	35	2.5 ± 0.1	3.9 ± 0.2	-7.93 ± 0.03	-32.9 ± 0.4	25.0 ± 0.4	0.97 ± 0.01
$p15^{32-111}$ ($\equiv p15^{\Delta N}$)	35	2.9 ± 0.2	3.5 ± 0.2	-7.87 ± 0.04	-33.8 ± 0.4	25.9 ± 0.5	1.01 ± 0.01
$p15^{50-77}$	25	5.56 ± 0.03	1.80 ± 0.01	-7.21± 0.01	-14.4 ± 0.1	7.2 ± 0.1	1.04 ± 0.01
	35	12.5 ± 0.8	0.8 ± 0.05	-7.00 ± 0.04	-17.7± 0.3	10.7 ± 0.5	1.05 ± 0.01
$p15^{59-70}$	35	83 ± 14	0.12 ± 0.02	-5.8 ± 0.1	-9.8 ± 0.1	4.0 ± 0.3	1

[a]Dissociation constant.
[b]Association constant.
[c]Standard free energy change of the association reaction.
[d]Standard enthalpy change of the association reaction.
[e]Standard entropy change of the association reaction multiplied by the absolute temperature.
[f]Stoichiometry (the number of p15 binding sites on a PCNA protomer), which was an adjustable parameter in the fitting of the experimental data with the exception of $p15^{59-70}$. For this peptide the value of *N* was set to 1, as the quality of the data did not allow for a reliable fitting of more than two independent parameters (the association constant and the enthalpy change).
The errors in the table are the fitting errors. Based on our previous experience with ITC measurements on several protein-protein interactions, we estimate that the experimental error in these measurements is around 5%.

Supplementary Table 2. Sequences of the oligonucleotides used for the DNA binding experiments.

DNA oligo	Sequence (5´-3´)
1 [a]	TCTGACTGC[iFluorT]GTCGGGCT[b]
2 [a]	AGCCCGACAGCAGTCAGAGCTTGCTAGGACGGACGGT
3 [a]	ACCGTCCGTCCTAGCAAGCATTTTTTT
4 [c]	TCAACATGATGTTCATAATCCCAA
5 [c]	TTGGGATTATGAACATCATGTTGA
6 [d]	CCTGCCTTACTTTTGGAAGAGAAA
7 [d]	TTTCTCTTCCAAAAGTAAGGCAGG
8 [e]	TTTTATACGATGGG
9 [e]	CCCATCGTAT

[a]The sequences of oligonucleotides 1-3 were taken from reference no. 26, where they were used to study the interaction with the archaeal *Sulfolobus sulfataricus* PCNA and the xeroderma pigmentosum complementation group F (XPF) nuclease homologues. The three oligonucleotides together form the flapped-DNA, and oligonucleotides 1 and 2 form the primed DNA.

[b][iFluorT] (internal fluorescein).

[c]Duplex used for the NMR analysis of the p15-DNA interaction.

[d]Duplex used for electron microscopy analysis.

[e]Sequences taken from reference no. 27 to generate the short primed DNA used for the NMR analysis of its interaction with PCNA (Supplementary Figure 10).